ACS Partner Journal

Journal of the American Society for Mass Spectrometry

pubs.acs.org/jasms

Article

Evaluation of Surface-Induced Dissociation Ion Mobility-Mass Spectrometry for Lipid Structural Characterization

Published as part of Journal of the American Society for Mass Spectrometry virtual special issue "Focus: Next Generation Mass Spectrometry Omics Technologies".

Rachel A. Harris, Jody C. May, Sophie R. Harvey, Vicki H. Wysocki, and John A. McLean*

Cite This: *J. Am. Soc. Mass Spectrom.* 2024, 35, 214−223

Read Online

ACCESS | Metrics & More | Article Recommendations | Supporting Information

Downloaded via OHIO STATE UNIV on February 7, 2024 at 19:58:42 (UTC).
See https://pubs.acs.org/sharingguidelines for options on how to legitimately share published articles.

ABSTRACT: The complexity of the lipidome has necessitated the development of novel analytical approaches for the identification and structural analysis of morphologically diverse classes of lipids. At this time, a variety of dissociation techniques have been utilized to probe lipid decomposition pathways in search of structurally diagnostic fragment ions. Here, we investigate the application of surface-induced dissociation (SID), a fragmentation technique that imparts energy to the target molecule via collision with a coated surface, for the fragmentation of seven lipids across four major lipid subclasses. We have developed a tuning methodology for guiding the efficient operation of a previously developed custom SID device for molecules as small as ca. 300 Da with ion mobility analysis of the fragmentation products. SID fragmentation of the various lipids analyzed was found to generate fragment ions similar to those observed in CID spectra, but fragment ion lab frame onset energies were lower in SID due to the higher energy deposition via a more massive target. For the largest lipid evaluated (cardiolipin 18:1), SID produced chain fragment ions, which yielded analytically useful information regarding the composition of the acyl tails. Ion mobility provided an orthogonal dimension of separation and aided in assigning product ions to their precursors. Overall, the combination of SID and IM-MS is another potential methodology in the analytical toolkit for lipid structural analysis.

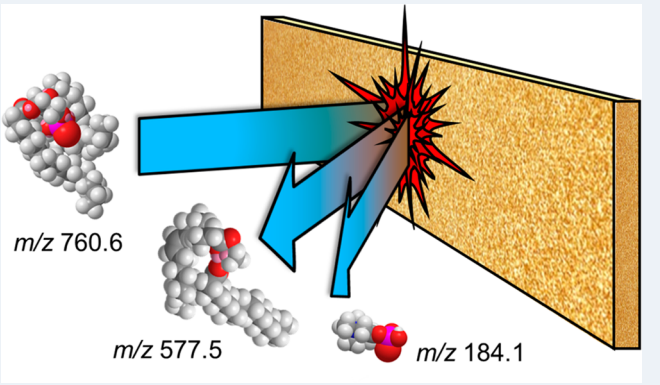

INTRODUCTION

The critical roles that lipids fulfill in both healthy and diseased biological systems have motivated the development of novel analytical strategies for lipid identification and quantitation.[1−3] However, the sheer quantity of unique lipids present in the lipidome, which is estimated to number in the tens of thousands,[4,5] and their inherent structural diversity, have historically made the task of analyzing lipids from biological samples daunting. Multiple review articles have recently been published discussing the current state of lipidomic research and the challenges that persist in the field.[6−8] While mass spectrometry (MS) continues to be the driving analytical technology for lipidomics, scientists have increasingly recognized the need to include additional analytical techniques with MS to provide a greater level of structural fidelity beyond what traditional MS-based fragmentation approaches, such as collision-induced dissociation (CID), can provide.[9,10] To that end, a plethora of alternative fragmentation strategies for lipid structural characterization have been developed over the years, including both generalized approaches that fragment the lipid analyte indiscriminately and more pinpointed approaches that target a specific lipid substructure or chemical bond. Examples of the former include transmission-type CID (referred to as higher energy CID, HCD, to contrast with ion trap CID)[11,12] and radical-based fragmentation strategies such as radical-directed dissociation (RDD),[13,14] electron impact excitation of ions from organics (EIEIO),[15,16] and ultraviolet photodissociation (UVPD).[17,18] Radical-based techniques, in particular, provide unique structural information due to their ability to induce fragmentation along the fatty acid chain. However, nontargeted mechanisms such as these often lead to very complex fragmentation spectra and low signal-to-noise ratios for diagnostic fragments, hampering their utility for the analysis of complex samples. Targeted approaches, on the other hand, involve specific ion−molecule reactions that are directed

Received: September 8, 2023
Revised: November 28, 2023
Accepted: December 5, 2023
Published: January 12, 2024

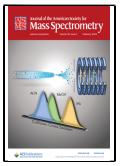

ACS Publications

© 2024 American Society for Mass Spectrometry. Published by American Chemical Society. All rights reserved.

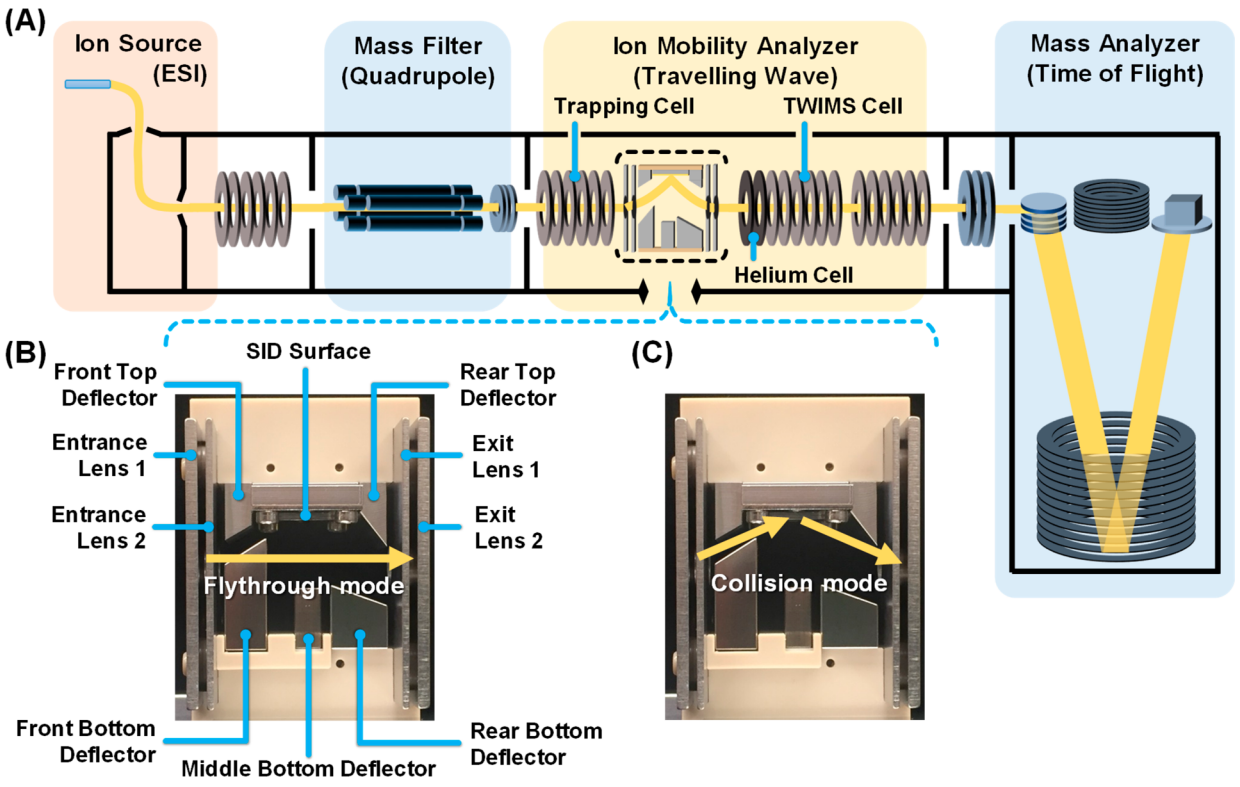

Figure 1. A schematic representation of the instrumentation used in this study. (A) A commercial Synapt G2 IM-MS was modified as described previously with a custom SID device installed in-line between the trap cell and the TWIMS cell. The SID device is controlled by adjusting the voltages on ten ion optical lenses and can be operated in (B) "Flythrough mode", in which lenses are tuned to pass ions through the device without collision with the surface, and (C) "Collision mode", in which the lenses are tuned to direct the ion beam toward the SID surface and resulting fragment ions are drawn through the exit lenses of the device and directed into the ion mobility stage of the instrument.

toward elucidating a particular region of the lipid, often the double bond position of the fatty acyl chains. Two commonly used techniques of this type include ozone-induced dissociation (Oz-ID)[19−21] and the Paternò−Büchi reaction (PB),[22−24] both of which ultimately induce fragmentation specifically at the lipid double bond. Each of these techniques has distinct advantages and disadvantages when applied to lipids, especially in the context of more complex biological samples. Thus far, no single analytical technique has been able to rapidly identify a given lipid to the highest level of structural specificity (i.e., headgroup class, acyl chain composition, *sn*-orientation, double bond position, and chirality), which indicates that novel, structurally specific fragmentation technologies are still needed. Moreover, an analytical platform combining multiple complementary techniques for lipid analysis will likely be necessary for the full structural characterization of lipids in biological samples.[25]

Surface-induced dissociation (SID) is a fragmentation technique originally developed by R. G. Cooks and co-workers in the 1980s for the analysis of small molecules because of limitations in mass spectrometers at the time.[26−30] In contrast to traditional CID fragmentation approaches, which occur via sequential collisions of the precursor molecule with a neutral background gas, SID imparts a large quantity of energy to the precursor through collision with a coated surface. Therefore, SID occurs on a faster reaction time scale compared to CID and can result in the dissociation proceeding via pathways consistent with an energy jump relative to multiple-collision CID dissociation mechanisms.[31,32] Thus, SID is potentially able to access fragmentation pathways unavailable to CID, as reported for protein complexes. Historically, the hardware implementation of SID was challenging due to the requirement that ions be directed onto a surface with remaining precursor and product ions collected and refocused for subsequent transfer to the MS stage. This required either extensive instrument modification or the design of new instrumental configurations for the explicit purpose of conducting SID experiments.[29,32−37] However, more recently, Wysocki and co-workers have developed SID devices that can be incorporated inline into commercial mass spectrometers, including the Waters Synapt G2 for experiments that combine SID and ion mobility-mass spectrometry (IM-MS) analysis.[38,39] The combination of SID and IM-MS has been primarily used to investigate the dissociation of protein supramolecular complexes and has demonstrated that SID of protein complexes sprayed under native-like conditions allows for the determination of the protein quaternary structure.[32,40,41] This stands in contrast to CID, which typically leads to the ejection of restructured, highly charged monomers.[32] This SID device was designed such that it could be incorporated downstream of the isolation quadrupole (Q) either before or after the ion mobility cell of the Synapt instrument (Q-SID-IM-MS and Q-IM-SID-MS, respectively), which allows for greater flexibility in designing experiments. Conducting the IM measurements before SID allows for the separation of isobaric ions (e.g., conformers or isomers) prior to fragmentation, which otherwise cannot be achieved with quadrupole isolation alone, whereas when IM is utilized after SID the structural analysis of the SID product ions can be achieved, which provides insight into specific dissociation pathways.

https://doi.org/10.1021/jasms.3c00319
J. Am. Soc. Mass Spectrom. 2024, 35, 214−223

In this work, we have developed a methodology for tuning and operating the SID device in the Q-SID-IM-MS configuration for small molecule analysis, in contrast to the large proteins and protein complexes typically studied with this device. To investigate the application of SID to relatively small-mass ions, seven lipid species across four lipid subclasses were analyzed via SID-IM-MS. Energy-resolved mass spectrometry (ERMS) and IM-MS spectra were utilized to examine lipid dissociation pathways and the structures of fragments generated.

EXPERIMENTAL METHODS

Sample Preparation. Lipid standards 1-hexadecanoyl-2-(9Z-octadecenoyl)-*sn*-glycero-3-phosphocholine (PC 16:0/18:1(9Z), 760 Da), 1-hexadecanoyl-2-(9Z-octadecenoyl)-*sn*-glycero-3-phosphoethanolamine (PE 16:0/18:1(9Z), 718 Da), 1-hexadecanoyl-2-(9Z-octadecenoyl)-*sn*-glycero-3-phosphoserine (PS 16:0/18:1, 761 Da), 1-hexadecanoyl-2-(9Z-octadecenoyl)-*sn*-glycero-3-phosphoglycerol (PG 16:0/18:1, 748 Da), 1′,3′-bis-[1,2-di(9Z-octadecenoyl)-*sn*-glycero-3-phospho]-*sn*-glycerol (CL 18:1(9Z)/18:1(9Z)/18:1(9Z)/18:1(9Z), 1455 Da), methyl (9Z)-octadecenoate (FA 18:1(9Z), 282 Da), and corticosterone (ST, 346 Da) were purchased from Avanti Polar Lipids and Cayman Chemical. Prior to analysis, samples were diluted to working concentrations ranging from 10 to 30 μM in 7:3 acetonitrile/water (Optima LC/MS grade, Fisher Scientific). Formic acid (0.1%, Optima grade, Fisher Scientific) was added to PC, PE, PS, PG, FA, and ST samples; 1 mM NaI (Fisher Scientific) was added to the PG sample; and 10 mM ammonium acetate (NH_4CH_3OOH, HPLC grade, Fluka, Honeywell) was added to the CL sample to promote the formation of $[M + H]^+$, $[M + Na]^+$, and $[M + NH_4]^+$ ion species, respectively. For mass calibration, 2 mg/mL NaI (Fisher Scientific) in 50:50 isopropyl alcohol/water (Optima LC/MS grade, Fisher) was utilized following Waters' recommended calibration protocols.

Instrumentation and SID Device Tuning. All experiments were performed on a Synapt G2 IM-MS instrument (Waters Corporation), modified with a custom SID device located between the trapping and mobility regions of the instrument (i.e., Q-SID-IM-MS) as described previously (Figure 1A).[38,40] In order to accommodate the device, the conventional trap cell traveling wave ion guide (TWIG) was exchanged for a trap cell with a truncated TWIG. The gold surface was prepared as previously reported[42] and consists of a thiolate self-assembled monolayer in which the final 10 (out of 12 total) carbon atoms are perfluorinated (FC_{12}). Collision with the surface was enabled by tuning each of the deflector lenses to optimize the SID ion activation. When SID was not utilized, a "flythrough" tuning strategy was used that allowed transmission of the ion beam through the SID device without surface collisions (Figure 1B). In this mode, a gentle voltage gradient was optimized for signal transmission from the trap, through the device, and into the helium cell and TWIMS cell with minimal activation; the voltages utilized for this tune permitted transmission of multiple small molecule lipid species, except for the cardiolipin sample, which required its own separate "flythrough" tune due to its significantly larger mass. Of note, switching between TOF only and IMTOF modes of the Synapt G2 raises the trap bias of the instrument by approximately ~43 eV; thus, three primary small molecule "flythrough" tunes were developed and utilized; the TOF-only mode was used solely to mass calibrate the instrument, while the IMTOF modes (small molecule and cardiolipin tunes, respectively) were used for all other experiments.

Tuning the SID device in the surface collision mode (Figure 1C) required optimizing the lenses for fragmentation for each compound analyzed. In general, collision mode tune files utilized approximately 30 additional volts applied to the deflector lenses in comparison with respective "flythrough" tune files to steer the ion beam into the surface and efficiently extract the resulting fragment ions. The laboratory frame collision energy for the SID is determined by the potential difference between the trap cell exit and the SID Surface. Therefore, to perform SID across a range of collision energies for these small molecules with this multi-lens device, the trap bias parameter was elevated to increase the potential difference between the trap exit and the surface and, concurrently, the entrance 1 and front bottom deflector lenses were increased by the same magnitude as the trap bias to maintain ion transmission through the device. As a consequence of altering only two of the device lenses when changing the SID collision energy, the signal transmission becomes increasingly deoptimized the further the collision energy is increased from the initial SID tune file. To address this issue, the SID optics were optimized at an intermediate collision energy (10 eV for FA, 30 eV for all other lipids), which was found to minimize ion transmission losses observed at the lowest and highest energies surveyed.

To date, most of the published work using this particular instrument configuration and the SID device has involved the analysis of large supramolecular protein complexes. As the IM-MS instrument utilizes buffer gases to improve ion transmission through the TWIG stages, it was necessary to minimize excess ion activation when transmitting ions from the source to the detector, as high ion transmission conditions can also lead to ion heating. In this study, it was observed that activation via incidental CID primarily occurred during post-SID ion injection into the TWIMS stage, defined as the potential difference between the SID surface and the helium cell. Ion activation occurred for IM injection energies of 20 eV or higher for the lipids analyzed in this study (Figure S1). By retuning the instrumental and SID device optics to minimize incidental CID imparted primarily during transfer into the He cell, the total fragment ion signal was reduced to less than 3% relative abundance of the precursor ion signal, except for four particularly labile lipids (PE, PS, CL, and FA) where the fragment ion signal was minimized to less than 10% to maintain sufficient precursor ion signal (>10 000 counts) to conduct ERMS studies. It is noted that incidental ion fragmentation was also observed on a separate IM-MS platform (Agilent 6560) even at a 0 V collision energy (Figure S2A), underscoring the facile dissociation propensity of lipids.

Experimental Parameters. All experiments were performed with the Synapt G2 operating in the IMTOF sensitivity mode, in which the quadrupole-isolated protonated precursor of PC 16:0/18:1 (m/z 760.6) exhibited a TOF-measured mass resolving power of approximately 25 000. The SID device was operated using an external power supply and custom software loaded on the G2 instrument control computer (Ardara Technologies, Ardara, PA). All samples were directly infused, and ESI source conditions were individually optimized for each lipid. Analyte ions were mass-isolated by the quadrupole (5 Da window) prior to either SID or CID. Both SID and CID fragmentation spectra were collected over a range of collision energies with post IM-MS analysis. IM traveling wave

https://doi.org/10.1021/jasms.3c00319
J. Am. Soc. Mass Spectrom. 2024, 35, 214−223

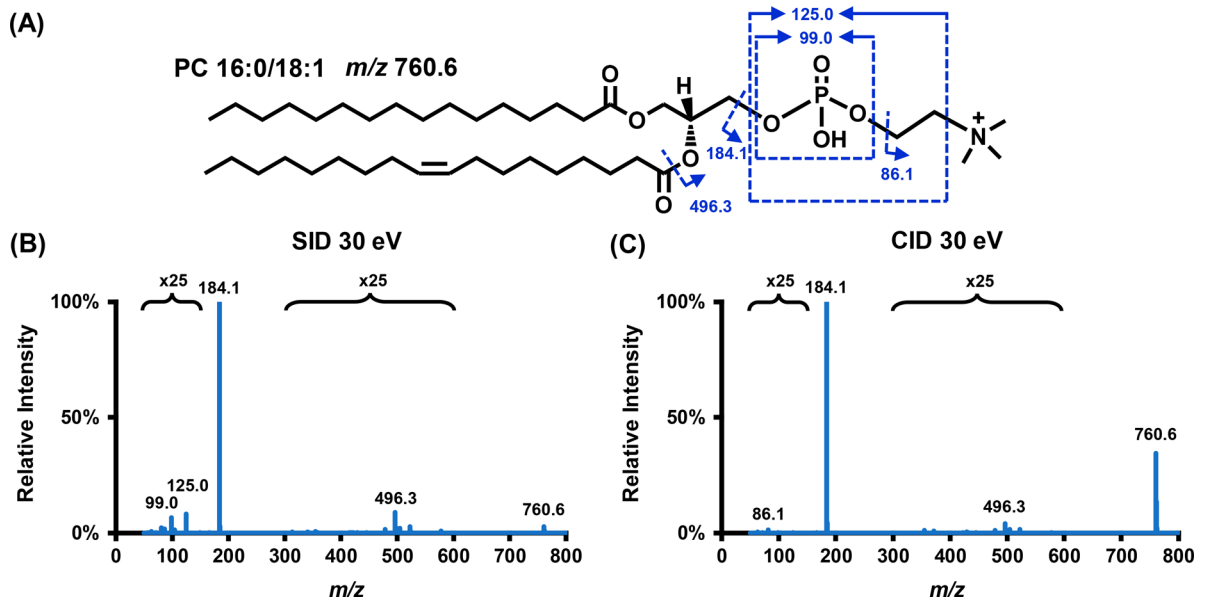

Figure 2. (A) Precursor molecule with selected product ions and their cleavage sites annotated. Comparison of the (B) SID and (C) CID fragmentation spectra of the lipid PC 16:0/18:1 at equivalent laboratory frame collision energies (30 eV). Dominant observed fragment ions are largely identical between the two fragmentation modalities, with the loss of the phosphocholine headgroup (m/z 184.1) serving as the dominant product ion arising from both ion activation modes.

conditions utilized the default settings (wave height of 40 V and wave velocity of 650 m/s) for all lipids except for ST (wave height of 35 V and wave velocity of 1000 m/s), which required different settings to disperse the fragment ions across the drift time space. The helium cell of the Synapt G2 serves to kinetically cool the ion beam prior to IM separation, allowing for increased nitrogen pressure in the TWIMS cell, which improves the ion mobility resolution.[43] Therefore, the helium cell was set at its maximal value of 200 mL/min for all samples except CL, in which the helium flow rate was lowered to 120 mL/min for more optimal signal transmission. Increasing the argon gas flow rate in the trapping cell and the nitrogen gas flow rate in the TWIMS cell was observed to increase the abundance of fragment ions arising from incidental CID. Therefore, these settings were decreased from their default settings to 0.4 mL/min argon and 60 mL/min nitrogen for all samples except CL, which instead used 1 mL/min argon and 40 mL/min nitrogen. For comparison with SID fragmentation spectra, CID was also performed at laboratory frame collision energies equivalent to those used in SID. All fragmentation experiments were performed in triplicate. Collision energies were stepped in increments of 10 eV for all lipids except PC and FA, for which steps were applied in 5 eV increments, and collision voltages were increased for several steps beyond the energy at which the precursor ion signal was fully depleted. The collision energy ranges for each lipid were as follows: PC 0−150 eV, PE 0−120 eV, PS 0−100 eV, PG 0−100 eV, FA 0−25 eV, CL 0−100 eV, and ST 0−50 eV. More detailed descriptions of experimental parameters can be found in the Supporting Information.

Data Analysis. All mass spectra were first processed in MassLynx v4.1 and Driftscope v2.5. Due to the large quantity of data generated (approximately 420 total data files), a custom C++ program was written to automate the data processing in MassLynx and subsequent exporting of each spectrum into Excel as a peak list at each collision energy. First, the direct infusion total ion chromatogram corresponding to each fragmentation energy was summed to produce an integrated mass spectrum. Next, the bottom 70% of the signal was omitted and the output was manually inspected to ensure only background ions were removed in this step, after which the remaining profile spectrum was smoothed and centroided (referred to as "centering" in the MassLynx software) to produce the final MS/MS spectrum. The default smoothing and centering settings in MassLynx were used, and centering was performed as a function of height rather than area. Then, the peak list and corresponding intensities were copied to Excel where the spectra were further processed using custom Excel VBA macros to remove all peaks above the mass of the precursor, remove centering artifact apodes, and convert the signal to relative intensity. Finally, an additional VBA macro was used to automatically generate energy-resolved mass spectra for the CID and SID fragmentation experiments of each lipid. This ERMS data were used to track the ions observed as a function of the laboratory frame collision energy in terms of relative abundance normalized to the summed ion abundance observed at each collision energy step.

RESULTS AND DISCUSSION

Direct Comparison of CID and SID Fragmentation Spectra. For initial characterization, a commonly studied phosphatidylcholine standard, PC 16:0/18:1(9Z), was utilized to tune the SID device for small molecule fragmentation. The structure of this lipid is depicted in Figure 2A, with observed cleavage sites and corresponding fragment ion m/z values annotated. Once a suitable SID tune was developed, the protonated lipid precursor at m/z 760.6 was isolated in the quadrupole and then subjected to SID activation at 30 eV (Figure 2B). For comparison, the lipid was also fragmented via CID at the same laboratory frame energy (Figure 2C). It was observed that the fragment ions were largely identical between the two fragmentation spectra, indicating that for a collision energy of 30 eV SID does not access any fragmentation pathways unavailable to CID, which is consistent with both

https://doi.org/10.1021/jasms.3c00319
J. Am. Soc. Mass Spectrom. 2024, 35, 214−223

SID and CID occurring by vibrational excitation. The dominant product ion in both spectra is the expected loss of the phosphocholine headgroup at m/z 184.1, while other low-abundance fragments include other headgroup fragments and the loss of the sn2 acyl chain at m/z 496.3. The major difference between the two fragmentation spectra is reflected in the differences in relative abundance of both the precursor ion and some of the low-mass fragment ions resulting from the sequential fragmentation of the headgroup. The precursor ion at m/z 760.6 is more substantially depleted in the SID fragmentation spectra, and the headgroup fragments at m/z 86.1, m/z 99.0, and m/z 125.0 are also increased in the SID fragmentation spectra relative to the CID fragmentation spectra. These observations are indicative of the fact that SID imparts more energy to the target molecule than CID at an equivalent laboratory frame energy because of the higher mass of the target, which is consistent with the literature and indicates the validity of the current SID tuning methodology.

Validation of Lipid Fragments using IM-MS Spectra and Kendrick Mass Defect Analysis. To identify lipid fragments unique to SID and therefore generated via dissociation pathways unavailable to CID at the same laboratory frame energy, SID and CID were performed over a range of collision energies for each of the lipid samples. Surveying a broad range of collision energies accounts for the fact that SID imparts more energy to the target molecule and allows for an interrogation of the entire chemical space of product ions that may be generated by each fragmentation pathway. The fragmentation of glycerophospholipids has been detailed thoroughly in the literature, particularly their dissociation via CID.[9,44] Therefore, elucidation of novel fragmentation mechanisms such as those potentially accessed via SID requires careful study of low-abundance fragment ions as well as those that appear at low m/z. Examination of IM-MS product ion spectra allows for facile inspection of low-intensity fragments by filtering out chemical noise for an improved signal-to-noise ratio, as well as enabling the identification of ions that fall within the same mobility−mass correlation region as other known fragments within the spectrum. Figure 3 compares SID (panel A) and CID (panel B) IM-MS fragmentation spectra for the PC 16:0/18:1 standard at a collision energy of 50 eV. As previously observed at 30 eV in Figure 2, most detected fragment ions, particularly those of significant signal intensity, are conserved between the two fragmentation modalities. These fragment ions labeled in Figure 3A correspond well to established fragmentation pathways for PC lipids. However, closer inspection of the IM-MS fragment ion spectra reveals additional details about the nature of the structure of the product ions. For example, the uncorrelated IM signal that manifests as vertical "streaking" at low m/z corresponds to ions that are formed during the TWIMS analysis due to metastable decay,[45] and this uncorrelated ion mobility signal is observed in both the SID and CID mobility spectra for several low-mass headgroup fragments, such as m/z 86.1, m/z 99.0, and m/z 125.0. More importantly, when IM separation occurs post-fragmentation, the mobility−mass correlations can be used to link product ions to their precursor(s). Specifically, these IM-MS trends allow for the isolation of product-specific mass and mobility spectra[46] and help validate whether a given ion results from the fragmentation of a specific precursor. As an example, both the SID and CID IM-MS fragmentation spectra depicted in Figure 3A and B exhibit two mobility-resolved ion signals at precursor

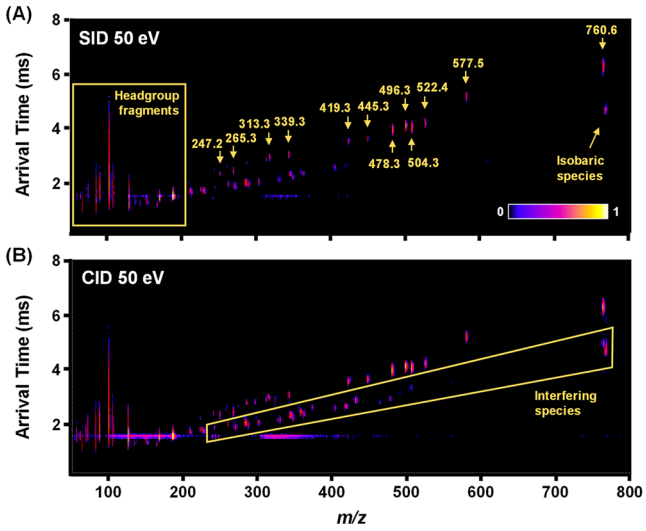

Figure 3. Comparison of the (A) SID and (B) CID IM-MS fragmentation spectra of the lipid PC 16:0/18:1 at the same lab frame collision energy (50 eV). As similarly observed in the MS fragmentation spectra in Figure 2, the detected fragment ions are largely identical between the two fragmentation modalities. The IM analysis in both ion activation modes reveals the presence of a series of interfering species, which resulted from transmission of multiple precursor ions within the quadrupole isolation window, but this isobaric interferent and related fragment ions partition in a distinct region of IM-MS space, labeled "interfering species" in panel B.

m/z 760.6, indicating that two distinct ion populations with different mobilities were isolated by the quadrupole. Postmobility CID (Figure S2B) indicated that only the higher arrival time feature corresponds in m/z and characteristic fragmentation to PC 16:0/18:1, whereas the second ion population at lower arrival time has both a different mass (m/z 763) and unexpected fragments. Both features are within the quadrupole isolation window used in this work (5 Da to increase the ion abundance of the isolated standard precursor) and both would be expected in a routine MS/MS experiment; however, the added IM dimension allows for the correct fragment ions to be isolated. The m/z fragment ions corresponding to this co-isolated ion appear along a different mobility−mass region in the post-CID/SID IM-MS analysis and are labeled as "interfering species" in Figure 3B. These interfering fragment ions and their precursor were not identified, but their location in mass mobility space below the known lipid and the isotopic distribution of the interfering precursor indicates that the species may be a higher order multimeric species.

Additional confidence in the assignment of SID product ions and interferents can be obtained using mass defect analysis of the high resolution (>20 000) mass measurements obtained on this platform. The mass defect refers to the change in mass due to the binding energy of nucleons, which is intrinsically related to the chemical composition of the analyte.[47,48] The Kendrick scale, which rescales the mass axis based on the mass of a CH_2 group (14 Da), is commonly used for relational analysis of molecules containing different CH_2 compositions, such as petroleum-based hydrocarbons and lipids.[49−51] In this case, Kendrick mass defect (KMD) analysis was applied to the 50 eV SID IM-MS spectrum of PC 16:0/18:1 shown in Figure 3A. The resulting KMD was plotted as a function of the exact mass, as shown in Figure 4A. Projecting the data in this manner

https://doi.org/10.1021/jasms.3c00319
J. Am. Soc. Mass Spectrom. 2024, 35, 214−223

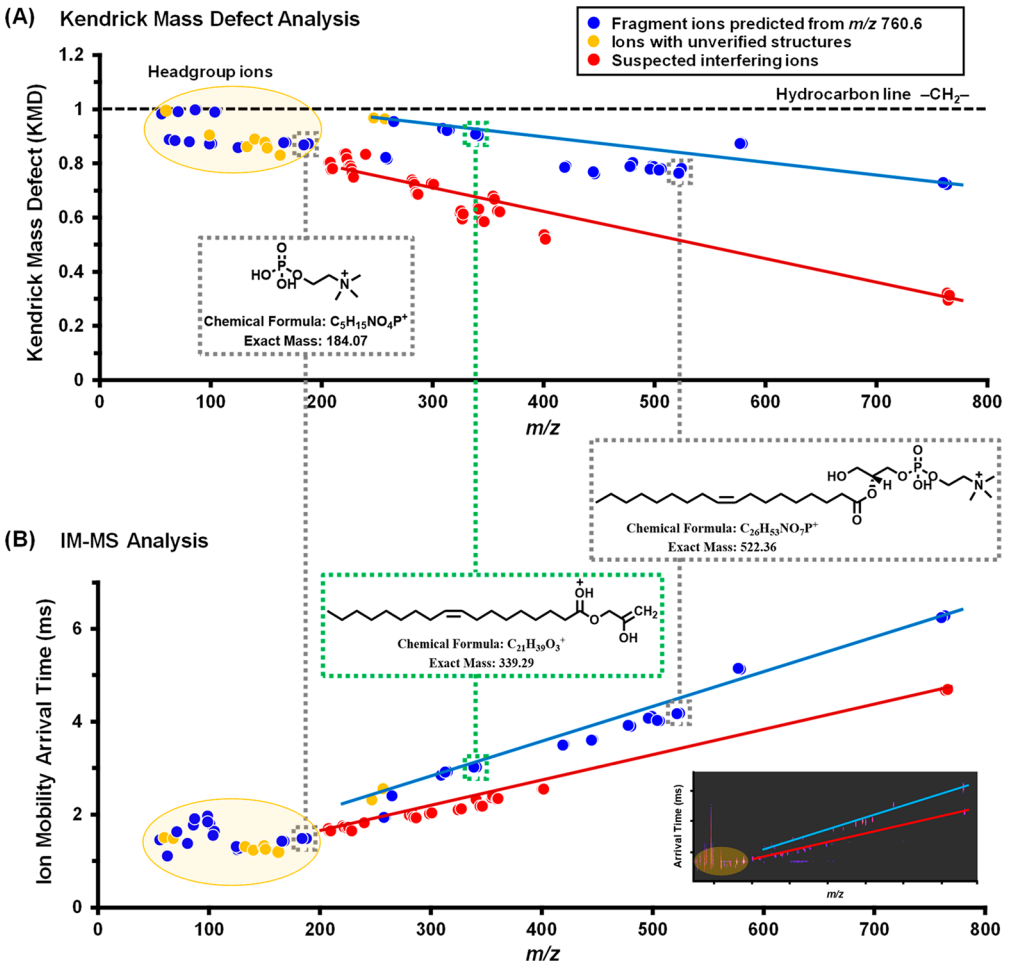

Figure 4. (A) Kendrick mass defect analysis of the fragment ions resulting from SID of PC 16:0/18:1 at 50 eV displays similar trends as observed in (B) the IM-MS mobility-mass correlation analysis. The blue trendline represents fragment ions resulting from the dissociation of the PC 16:0/18:1 precursor at m/z 760.6. Blue markers represent fragment ions with chemical formulas and structures verified to result from known PC fragmentation pathways, whereas orange markers represent ions with unverified formulas and structures. As previously observed in Figure 3, the red trendline represents fragment ions resulting from an interfering species that is introduced during quadrupole isolation of m/z 760.6. The circled region at low m/z contains ions arising from postmobility dissociation (vertical "streaking" in the inset) as well as ions that are not observed to mobility separate (i.e., surfing ions) under the TW conditions used.

resulted in two distinct trendlines of ions, highlighted in blue and red on the figure, as well as a cluster of ions at low m/z (circled region) that correspond predominantly to known lipid headgroup fragments only partially separated in TWIMS due to "ion surfing" behavior.[52] Of note is that these two trendlines in KMD analysis resemble the ion mobility–mass correlations that are plotted in Figure 4B for the same data. Comparing the two plots in Figure 4 leads to the conclusion that the two trendlines in the KMD analysis correspond to both ions from SID of the primary precursor and ions of unknown origin, which may include multiply charged multimers co-isolated in the quadrupole. These interfering species lie lower in KMD space than the lipid precursor and its confirmed fragments, indicating that they have a lower CH_2 content than the species of interest. Thus, KMD analysis provides complementary chemical information as IM-MS correlations in that both align chemically similar fragment ions into distinct regions of space.

The combined IM-MS and KMD analyses were subsequently applied to the SID activation of a different lipid: PG 16:0/18:1 (sodiated m/z 771.5). Unlike the previous example, this second lipid exhibits several unique ions at high SID collision energies (>70 eV) that were not detected in the complementary CID spectra (Figure S3) and thus were not initially suspected to originate from higher-charge-state multimers. Analysis of the SID IM-MS spectra of product ions suggested that the unique SID-derived ions in question (m/z 284.3, m/z 340.4, and m/z 368.4) appear slightly higher than the region containing known PG lipid fragment ions; however the mobility–mass correlations are not well-defined (Figure S4A). However, KMD analysis revealed that the ions in question did not correlate in KMD space with other known fragments, indicating that they likely did not result from the SID of the sodiated PG 16:0/18:1 precursor at m/z 771.51 (Supplementary Figure S4). Moreover, all three of the ions of interest (m/z 284.3, m/z 340.4, and m/z 368.4) possessed KMD values that were very close to the hydrocarbon limit of 1 (0.987, 0.987, and 0.988, respectively), which indicated that theses ions were potentially hydrocarbon interferents only observed at high SID collision energies. To further investigate the source of these interfering ions, a follow-up experiment was conducted at The Ohio State University, where the same PG lipid was subjected to SID fragmentation on a separate IM-MS system (also a Synapt G2) using a freshly prepared SID fluorocarbon surface. The two spectra obtained at equivalent

https://doi.org/10.1021/jasms.3c00319
J. Am. Soc. Mass Spectrom. 2024, 35, 214–223

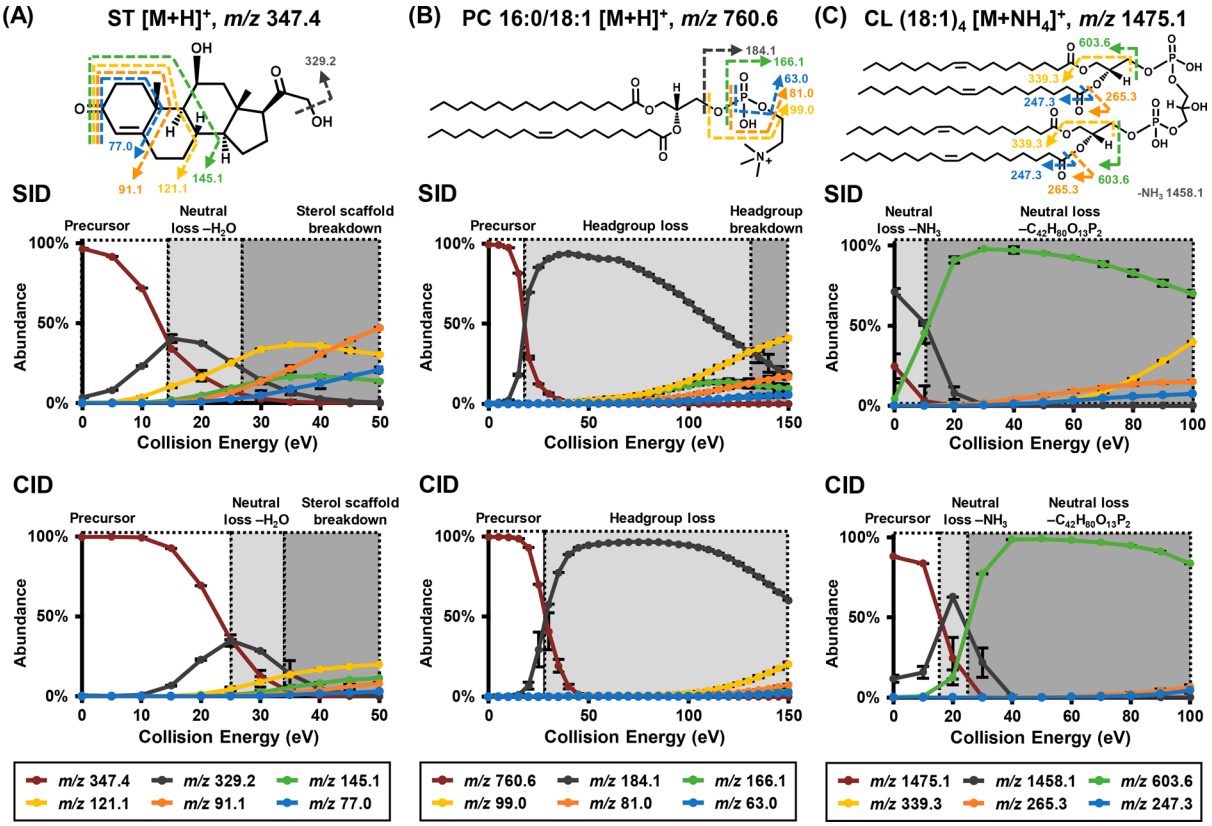

Figure 5. Relative ion intensity of precursor and predominant fragment ions as a function of the laboratory frame collision energy for (A) corticosterone ST, (B) PC 16:0/18:1, and (C) CL $(18:1)_4$ for both SID (upper plots) and CID (lower plots). Shaded areas of each ERMS ion breakdown curve correspond to precursor species (white), first-generation fragments (light gray), and second-generation fragments (dark gray). Because SID exhibits more efficient energy deposition to the molecule, the onset of precursor fragmentation and further structural decomposition occur at lower collision energies relative to CID.

SID fragmentation energies of 100 eV are shown in Figure S5. First, the SID results from the fresh surface exhibit a higher abundance of lower m/z ions, suggesting more efficient ion activation. Importantly, the three ions of questionable origin were not detected when SID was performed on a freshly installed fluorinated gold surface, further supporting the assertion that these ions are unrelated to the PG lipid. It is hypothesized that these interfering ions are hydrocarbon contaminants introduced to the surface during the routine process of venting the instrument for this earlier-generation IM-MS platform, emphasizing the importance of maintaining a clean surface for unambiguous SID results (e.g., the Wysocki laboratory recommends changing surfaces with each instrument vent). However, the use of orthogonal analytical strategies such as ion mobility and mass defect analyses enabled the discrimination of these contaminant ions from authentic SID fragment ions originating from the precursor.

Comparison of Energy-Resolved CID and SID. Once the product ions of each of the seven lipids were verified via IM-MS and KMD analyses, the relative intensities of the most abundant fragment ions were plotted as a function of the laboratory frame collision energy to generate energy-resolved mass spectra (ERMS). ERMS measurements provide insight into the major decomposition pathways as the activation energy increases. The ERMS results for three selected lipids are depicted in Figure 5 for corticosterone (ST), PC 16:0/18:1, and CL $(18:1)_4$. For all lipids analyzed, it was observed that as the mass of the lipid precursor increased, the energy required to induce fragmentation also increased, which is a feature common to collision-based fragmentation techniques that follow the general statistical theory of mass spectrometry. Additionally, the most abundant product ions are common between SID and CID fragmentation mechanisms for all three lipids depicted in Figure 5, as well as in ERMS for the other four lipids (Figures S6–S12). However, the collision energies at which each fragment ion appears are lower in SID versus CID. This can be seen in the relative transitions from one dominant species in the mass spectra to another (annotated as shaded regions in the ERMS plots). It should be emphasized, however, that ERMS comparisons between SID and CID are based on laboratory frame collision energies rather than center-of-mass (E_{COM}) because there does not exist a simple means of determining the internal energy deposition in the fragmentation of lipids. In the past, various approaches such as energy calibration against thermometer ion data have been utilized to characterize CID and SID energy deposition for small molecules; however, the "effective" mass of the surface, which is needed to calculate the E_{COM} for surface collision, appears to depend on several factors, including the nature of the projectile ion as well as the composition of the surface.[31,53] Therefore, comparisons of the laboratory frame collision energy between SID and CID are not intended to imply the same energy deposition but still provide qualitatively useful information regarding overall differences in energy deposition between the two processes.

The largest differences between SID and CID ERMS measurements occurred at the highest collision energies surveyed. For example, SID was observed to deplete the signal

https://doi.org/10.1021/jasms.3c00319
J. Am. Soc. Mass Spectrom. 2024, 35, 214–223

Table 1. Comparison of Laboratory Frame Collision Energies at 50% Precursor Depletion in SID vs CID for Selected Lipids

	PC		PE		PS		PG		FA		CL		ST	
	SID	CID	SID	CID	SID	CID	SID	CID	SID	CID	SID	CID	SID	CID
precursor ΔU_{50} (eV)[a]	18	32	15	25	9	24	35	37	3	18	<0	19	23	32

[a]The ΔU_{50} denotes the lab frame collision energy at which 50% of the precursor species has been depleted.

of the headgroup of PC 16:0/18:1 (m/z 184.1) by ca. 55% of the maximum SID collision energy surveyed (150 eV), whereas the headgroup ion signal was only depleted by ca. 20% at the maximum CID energy surveyed (180 eV, Figure S6). The other glycerophospholipids surveyed behaved similarly to PC 16:0/18:1, with higher SID energies leading to the production of small headgroup fragments that were only minimally observed via CID fragmentation. Additionally, the CL spectra begin to exhibit smaller ion fragments (m/z 247.3, m/z 265.3, and m/z 339.3) at approximately 70 eV via SID, while these ions only appear at ca. 100 eV when performing CID and only at low abundance. To characterize the comparison of the two fragmentation techniques for the lipids analyzed, the collision energy at which 50% of a species has been depleted (ΔU_{50}), was determined for the precursor ions. This information is summarized in Table 1 and complements the ERMS breakdown plots. The ΔU_{50} for precursor ions was always lower for SID relative to CID for the lipids analyzed, indicating that SID is a more efficient fragmentation mechanism. Together, these observations provide additional support that SID deposits greater energy to the analyte molecule than CID at a given lab frame collision energy in the current instrumental configuration, which is supported by theory and prior results in the literature.[26,31,54]

Aside from the differences in fragment ion appearance and depletion energies between the two dissociation techniques, only minor differences were observed for ERMS of the chosen lipids. For example, the formation of m/z 166.1 (a headgroup fragment) is preferred over the formation of m/z 81.0 (another headgroup fragment) in the fragmentation of PC 16:0/18:1 for SID relative to CID (see Figure S6 for a clearer representation of this observation), but otherwise no fragment ions unique to SID were detected for this lipid or the other lipids analyzed in this study. Cheng and Gross have previously discussed that, under high-energy CID conditions, lipid chain fragments with 14 Da spacing are observed for a variety of lipids.[55] These charge remote lipid-tail informative fragments are absent in single-stage keV CID and in our eV CID and SID data for PCs, for example, although we could likely see them from another stage of fragmentation, as noted in the Gross review. We note that the ability of SID to access higher-energy fragment ion channels provides analytical benefits to the larger lipids, such as the case with CL where several chain fragments are observed in the ERMS data (Figure 5C). These observations suggest that, although SID imparts greater energy to the analyte in the dissociation process, smaller molecules such as the majority of lipids may not possess additional higher-energy fragmentation pathways that are otherwise inaccessible to CID or that the fragments that are formed are kinetically preferred by CID and SID, as has been reported previously for peptide fragmentation.[56] Low-mass, singly charged CsI clusters show similar results with CID and SID, while higher m/z clusters give dramatically different fragmentation pathways with CID and SID.[57] In contrast to small molecules, larger analytes such as protein complexes undergo restructuring caused by the many low-energy collisions of multistep CID, whereas they dissociate at the weakest noncovalent bonds via the higher-energy jump provided by SID. For these reasons, the lack of unique SID fragments in these small molecule experiments is justifiable, though we also note that simplified manual acquisition over the wide energy range surveyed involved using broadly optimized SID parameters, which may have resulted in lower abundance fragment ions being overlooked in these surveys. For the lipids in this study, most of the differences between SID and CID in the ERMS occurred at high collision energies, with very small headgroup fragments (<m/z 100) that are not particularly useful for structural identification; however, other classes of low m/z molecules could still potentially benefit from the large energy deposition provided by SID. Although SID was not found to generate novel fragment ions or fragmentation pathways for the lipids analyzed in this study, it remains a useful technique due to its high fragmentation efficiency and ability to generate fragments at lower laboratory frame collision energies.

CONCLUSIONS

Surface-induced dissociation (SID) was used to fragment seven different lipid molecules representing four different lipid subclasses. For the range of small molecule lipids analyzed in this study (ca. 300−1500 Da), SID was found to produce fragmentation spectra comparable to those of traditional CID activation. However, SID promoted more fragmentation at the same laboratory frame energy, which yielded more in-depth structural information, particularly regarding the lipid headgroup of glycerophospholipids. The use of IM separations following SID fragmentation provided additional structural information for the generated product ions, and mobility−mass correlation trends combined with mass defect analysis revealed the presence of interferent ions and aided in the assignment of product ions to the correct precursor species. Finally, energy-resolved mass spectra indicated that fragment ions appear at lower collision energies in SID compared to CID, which supports our current understanding that SID deposits a greater quantity of energy to the target molecule in comparison to CID at the same lab frame collision energy. SID serves as another important analytical technique in the toolkit for lipid structural analysis, particularly when combined with IM-MS analysis and interpreted with multidimensional correlation strategies, such as mobility−mass and mass defect analysis.

ASSOCIATED CONTENT

Supporting Information

The Supporting Information is available free of charge at https://pubs.acs.org/doi/10.1021/jasms.3c00319.

Tabulated instrument parameters, mass spectra results from minimizing incident ion activation, extraction of IM-resolved fragmentation spectra, post-IM CID of PC 16:0/18:1, detailed results for PG 16:0/18:1 (CID/SID spectral comparisons, IM-MS, and KMD analysis), and ERMS results for all seven lipids in this study (PDF)

https://doi.org/10.1021/jasms.3c00319
J. Am. Soc. Mass Spectrom. 2024, 35, 214−223

AUTHOR INFORMATION

Corresponding Author

John A. McLean − *Department of Chemistry, Center for Innovative Technology, Vanderbilt Institute of Chemical Biology, Vanderbilt Institute for Integrative Biosystems Research and Education, Vanderbilt University, Nashville, Tennessee 37235, United States;* orcid.org/0000-0001-8918-6419; Email: john.a.mclean@vanderbilt.edu

Authors

Rachel A. Harris − *Department of Chemistry, Center for Innovative Technology, Vanderbilt Institute of Chemical Biology, Vanderbilt Institute for Integrative Biosystems Research and Education, Vanderbilt University, Nashville, Tennessee 37235, United States;* orcid.org/0000-0001-7728-1187

Jody C. May − *Department of Chemistry, Center for Innovative Technology, Vanderbilt Institute of Chemical Biology, Vanderbilt Institute for Integrative Biosystems Research and Education, Vanderbilt University, Nashville, Tennessee 37235, United States;* orcid.org/0000-0003-4871-5024

Sophie R. Harvey − *Department of Chemistry and Biochemistry, The Ohio State University, Columbus, Ohio 43210, United States;* orcid.org/0000-0003-0763-8173

Vicki H. Wysocki − *Department of Chemistry and Biochemistry, The Ohio State University, Columbus, Ohio 43210, United States;* orcid.org/0000-0003-0495-2538

Complete contact information is available at: https://pubs.acs.org/10.1021/jasms.3c00319

Notes

The authors declare no competing financial interest.

ACKNOWLEDGMENTS

The authors would like to thank Kevin Giles and Waters Corporation for detailed conversations regarding the application and installation of SID on the Waters Synapt instrument platform. This work was supported in part using the resources of the Center for Innovative Technology at Vanderbilt University and NIH funding to V.H.W. (P41GM128577). R.H. acknowledges the Harold Stirling Graduate Fellowship from the Vanderbilt University Graduate School. Financial support for Vanderbilt authors were provided by the U.S. Department of Energy, Office of Science (DOE SC) under award number DE-SC0019404 and the U.S. Environmental Protection Agency (EPA) under Grant R839504. This work has not been formally reviewed by the EPA, and the EPA does not endorse any products or commercial services mentioned in this document. The views and conclusions contained in this document are those of the authors and should not be interpreted as representing the official policies, either expressed or implied, of the U.S. Government.

REFERENCES

(1) Wenk, M. R. The Emerging Field of Lipidomics. *Nat. Rev. Drug Discovery* **2005**, *4* (7), 594−610.

(2) Blanksby, S. J.; Mitchell, T. W. Advances in Mass Spectrometry for Lipidomics. *Ann. Rev. Anal. Chem.* **2010**, *3* (1), 433−465.

(3) Rolim, A. E. H.; Henrique-Araújo, R.; Ferraz, E. G.; de Araújo Alves Dultra, F. K.; Fernandez, L. G. Lipidomics in the Study of Lipid Metabolism: Current Perspectives in the Omic Sciences. *Gene* **2015**, *554* (2), 131−139.

(4) Schuster, S.; Fichtner, M.; Sasso, S. Use of Fibonacci Numbers in Lipidomics − Enumerating Various Classes of Fatty Acids. *Sci. Rep.* **2017**, *7*, 39821.

(5) Wishart, D. S; Feunang, Y. D.; Marcu, A.; Guo, A. C.; Liang, K.; Vázquez-Fresno, R.; Sajed, T.; Johnson, D.; Li, C.; Karu, N.; Sayeeda, Z.; Lo, E.; Assempour, N.; Berjanskii, M.; Singhal, S.; Arndt, D.; Liang, Y.; Badran, H.; Grant, J.; Serra-Cayuela, A.; Liu, Y.; Mandal, R.; Neveu, V.; Pon, A.; Knox, C.; Wilson, M.; Manach, C.; Scalbert, A. HMDB 4. 0 : The Human Metabolome Database for 2018. *Nucleic Acids Res.* **2018**, *46* (D1), D608−D617.

(6) Harris, R. A.; Leaptrot, K. L.; May, J. C.; McLean, J. A. New Frontiers in Lipidomics Analyses Using Structurally Selective Ion Mobility-Mass Spectrometry. *TrAC - Trends Anal. Chem.* **2019**, *116*, 316−323.

(7) Hancock, S. E.; Poad, B. L. J.; Batarseh, A.; Abbott, S. K.; Mitchell, T. W. Advances and Unresolved Challenges in the Structural Characterization of Isomeric Lipids. *Anal. Biochem.* **2017**, *524*, 45−55.

(8) Zheng, X.; Smith, R. D.; Baker, E. S. Recent Advances in Lipid Separations and Structural Elucidation Using Mass Spectrometry Combined with Ion Mobility Spectrometry, Ion−Molecule Reactions and Fragmentation Approaches. *Curr. Opin. Chem. Biol.* **2018**, *42*, 111−118.

(9) Pulfer, M.; Murphy, R. C. Electrospray Mass Spectrometry of Phospholipids. *Mass Spectrom. Rev.* **2003**, *22* (5), 332−364.

(10) Ivanova, P. T.; Milne, S. B.; Byrne, M. O.; Xiang, Y.; Brown, H. A. Glycerophospholipid Identification and Quantitation by Electrospray Ionization Mass Spectrometry. *Methods Enzymol.* **2007**, *432* (07), 21−57.

(11) Pittenauer, E.; Allmaier, G. The Renaissance of High-Energy CID for Structural Elucidation of Complex Lipids : MALDI-TOF/RTOF-MS of Alkali Cationized Triacylglycerols. *J. Am. Soc. Mass Spectrom.* **2009**, *20*, 1037−1047.

(12) Bird, S. S.; Marur, V. R.; Sniatynski, M. J.; Greenberg, H. K.; Kristal, B. S. Serum Lipidomics Profiling Using LC-MS and High Energy Collisional Dissociation Fragmentation: Focus on Triglyceride Detection and Characterization. *Anal. Chem.* **2011**, *83* (17), 6648−6657.

(13) Pham, H. T.; Ly, T.; Trevitt, A. J.; Mitchell, T. W.; Blanksby, S. J. Differentiation of Complex Lipid Isomers by Radical-Directed Dissociation Mass Spectrometry. *Anal. Chem.* **2012**, *84* (17), 7525−7532.

(14) Pham, H. T.; Julian, R. R. Radical Delivery and Fragmentation for Structural Analysis of Glycerophospholipids. *Int. J. Mass Spectrom.* **2014**, *370*, 58−65.

(15) Campbell, J. L.; Baba, T. Near-Complete Structural Characterization of Phosphatidylcholines Using Electron Impact Excitation of Ions from Organics. *Anal. Chem.* **2015**, *87* (11), 5837−5845.

(16) Baba, T.; Campbell, J.L.; Le Blanc, J. C. Y.; Baker, P. S.; Ikeda, K. Quantitative Structural Multiclass Lipidomics Using Differential Mobility : Electron Impact Excitation of Ions from Organics (EIEIO) Mass Spectrometry. *J. Lipid Res.* **2018**, *59*, 910−919.

(17) Klein, D. R.; Brodbelt, J. S. Structural Characterization of Phosphatidylcholines Using 193 nm Ultraviolet Photodissociation Mass Spectrometry. *Anal. Chem.* **2017**, *89* (3), 1516−1522.

(18) Ryan, E.; Nguyen, C. Q. N.; Shiea, C.; Reid, G. E. Detailed Structural Characterization of Sphingolipids via 193 nm Ultraviolet Photodissociation and Ultra High Resolution Tandem Mass Spectrometry. *J. Am. Soc. Mass Spectrom.* **2017**, *28* (7), 1406−1419.

(19) Thomas, M. C.; Mitchell, T. W.; Harman, D. G.; Deeley, J. M.; Nealon, J. R.; Blanksby, S. J. Ozone-Induced Dissociation: Elucidation of Double Bond Position within Mass-Selected Lipid Ions. *Anal. Chem.* **2008**, *80* (1), 303−311.

(20) Kozlowski, R. L.; Campbell, J. L.; Mitchell, T. W.; Blanksby, S. J. Combining Liquid Chromatography with Ozone-Induced Dissociation for the Separation and Identification of Phosphatidylcholine Double Bond Isomers. *Anal. Bioanal. Chem.* **2015**, *407* (17), 5053−5064.

(21) Marshall, D. L.; Pham, H. T.; Bhujel, M.; Chin, J. S. R.; Yew, J. Y.; Mori, K.; Mitchell, T. W.; Blanksby, S. J. Sequential Collision- and

Ozone-Induced Dissociation Enables Assignment of Relative Acyl Chain Position in Triacylglycerols. *Anal. Chem.* **2016**, *88* (5), 2685−2692.
(22) Ma, X.; Xia, Y. Pinpointing Double Bonds in Lipids by Paternò-Büchi Reactions and Mass Spectrometry. *Angew. Chem., Int. Ed.* **2014**, *53* (10), 2592−2596.
(23) Ma, X.; Zhao, X.; Li, J.; Zhang, W.; Cheng, J. X.; Ouyang, Z.; Xia, Y. Photochemical Tagging for Quantitation of Unsaturated Fatty Acids by Mass Spectrometry. *Anal. Chem.* **2016**, *88* (18), 8931−8935.
(24) Zhang, W.; Zhang, D.; Chen, Q.; Wu, J.; Ouyang, Z.; Xia, Y. Online Photochemical Derivatization Enables Comprehensive Mass Spectrometric Analysis of Unsaturated Phospholipid Isomers. *Nat. Commun.* **2019**, *10* (1), 1−9.
(25) Zhang, W.; Jian, R.; Zhao, J.; Liu, Y.; Xia, Y. Deep-Lipidotyping by Mass Spectrometry: Recent Technical Advances and Applications. *J. Lipid Res.* **2022**, *63* (7), 100219.
(26) Mabud, M. A.; Dekrey, M. J.; Cooks, R. G. Surface-Induced Dissociation of Molecular Ions. *Int. J. Mass Spectrom. Ion Processes* **1985**, *67* (3), 285−294.
(27) Cooks, R. G.; Ast, T.; Mabud, M. A. Collisions of Polyatomic Ions with Surfaces. *Int. J. Mass Spectrom. Ion Processes* **1990**, *100*, 209−265.
(28) Hayward, M. J.; Mabud, M. A.; Cooks, R. G. Ion/Surface Collisions for Distinction of Isomeric $[C_6H_6]^+$ and $[C_6H_6]^{2+}$ Ions. *J. Am. Chem. Soc.* **1988**, *110* (5), 1343−1346.
(29) Grill, V.; Shen, J.; Evans, C.; Cooks, R. G. Collisions of Ions with Surfaces at Chemically Relevant Energies: Instrumentation and Phenomena. *Rev. Sci. Instrum.* **2001**, *72* (8), 3149−3179.
(30) Wysocki, V. H.; Kenttämaa, H. I.; Cooks, R. G. Internal Energy Distributions of Isolated Ions after Activation by Various Methods. *Int. J. Mass Spectrom. Ion Processes* **1987**, *75* (2), 181−208.
(31) Wysocki, V. H.; Joyce, K. E.; Jones, C. M.; Beardsley, R. L. Surface-Induced Dissociation of Small Molecules, Peptides, and Non-Covalent Protein Complexes. *J. Am. Soc. Mass Spectrom.* **2008**, *19* (2), 190−208.
(32) Snyder, D. T.; Harvey, S. R.; Wysocki, V. H. Surface-induced Dissociation Mass Spectrometry as a Structural Biology Tool. *Chem. Rev.* **2022**, *122* (8), 7442−7487.
(33) Schey, K. L.; Durkin, D. A.; Thornburg, K. R. Design and Performance of an In-Line Surface-Induced Dissociation Device in a Four-Sector Mass Spectrometer. *J. Am. Soc. Mass Spectrom.* **1995**, *6* (4), 257−263.
(34) Bier, M. E.; Schwartz, J. C.; Schey, K. L.; Cooks, R. G. Tandem Mass Spectrometry Using an In-Line Ion-Surface Collision Device. *Int. J. Mass. Spectrom. Ion Processes* **1990**, *103*, 1−19.
(35) Snyder, D. T.; Panczyk, E. M.; Somogyi, A.; Kaplan, D. A.; Wysocki, V. H. Simple and Minimally Invasive SID Devices for Native Mass Spectrometry. *Anal. Chem.* **2020**, *92* (16), 11195−11203.
(36) Sun, W.; May, J. C.; Russell, D. H. A Novel Surface-Induced Dissociation Instrument for Ion Mobility-Time-of-Flight Mass Spectrometry. *Int. J. Mass Spectrom.* **2007**, *259* (1−3), 79−86.
(37) Sun, W.; May, J. C.; Gillig, K. J.; Russell, D. H. A Dual Time-of-Flight Apparatus for an Ion Mobility-Surface-Induced Dissociation-Mass Spectrometer for High-Throughput Peptide Sequencing. *Int. J. Mass Spectrom.* **2009**, *287* (1−3), 39−45.
(38) Zhou, M.; Huang, C.; Wysocki, V. H. Surface-Induced Dissociation of Ion Mobility-Separated Noncovalent Complexes in a Quadrupole/Time-of-Flight Mass Spectrometer. *Anal. Chem.* **2012**, *84* (14), 6016−6023.
(39) Snyder, D. T.; Jones, B. J.; Lin, Y.-F.; Cooper-Shepherd, D. A.; Hewitt, D.; Wildgoose, J.; Brown, J. M.; Langridge, J. I.; Wysocki, V. H. Surface-Induced Dissociation of Protein Complexes on a Cyclic Ion Mobility Spectrometer. *Analyst* **2021**, *146*, 6861−6873.
(40) Zhou, M.; Dagan, S.; Wysocki, V. H. Impact of Charge State on Gas-Phase Behaviors of Noncovalent Protein Complexes in Collision Induced Dissociation and Surface Induced Dissociation. *Analyst* **2013**, *138* (5), 1353−1362.
(41) Song, Y.; Nelp, M. T.; Bandarian, V.; Wysocki, V. H. Refining the Structural Model of a Heterohexameric Protein Complex: Surface Induced Dissociation and Ion Mobility Provide Key Connectivity and Topology Information. *ACS Cent. Sci.* **2015**, *1* (9), 477−487.
(42) Harvey, S. R.; Seffernick, J. T.; Quintyn, R. S.; Song, Y.; Ju, Y.; Yan, J.; Sahasrabuddhe, A. N.; Norris, A.; Zhou, M.; Behrman, E. J.; Lindert, S.; Wysocki, V. H. Relative Interfacial Cleavage Energetics of Protein Complexes Revealed by Surface Collisions. *Proc. Natl. Acad. Sci. U.S.A.* **2019**, *116* (17), 8143−8148.
(43) Giles, K.; Williams, J. P.; Campuzano, I. Enhancements in Travelling Wave Ion Mobility Resolution. *Rapid Commun. Mass Spectrom.* **2011**, *25* (11), 1559−1566.
(44) Murphy, R. C.; Axelsen, P. H. Mass Spectrometric Analysis of Long-Chain Lipids. *Mass Spectrom. Rev.* **2011**, *30* (4), 579−599.
(45) Rose, B. S.; Leaptrot, K. L.; Harris, R. A.; Sherrod, S. D.; May, J. C.; McLean, J. A. High Confidence Shotgun Lipidomics Using Structurally Selective Ion Mobility-Mass Spectrometry. *Methods Mol. Biol.* **2021**, *2306*, 11−37.
(46) Harris, R. A.; May, J. C.; Stinson, C. A.; Xia, Y.; McLean, J. A. Determining Double Bond Position in Lipids Using Online Ozonolysis Coupled to Liquid Chromatography and Ion Mobility-Mass Spectrometry. *Anal. Chem.* **2018**, *90* (3), 1915−1924.
(47) May, J. C.; McLean, J. A. Advanced Multidimensional Separations in Mass Spectrometry: Navigating the Big Data Deluge. *Ann. Rev. Anal. Chem.* **2016**, *9* (1), 387−409.
(48) Sleno, L. The Use of Mass Defect in Modern Mass Spectrometry. *J. Mass Spectrom.* **2012**, *47* (2), 226−236.
(49) Kendrick, E. A Mass Scale Based on CH_2 = 14.0000 for High Resolution Mass Spectrometry of Organic Compounds. *Anal. Chem.* **1963**, *35* (13), 2146−2154.
(50) Hughey, C. A.; Hendrickson, C. L.; Rodgers, R. P.; Marshall, A. G.; Qian, K. Kendrick Mass Defect Spectrum: A Compact Visual Analysis for Ultrahigh-Resolution Broadband Mass Spectra. *Anal. Chem.* **2001**, *73* (19), 4676−4681.
(51) Lerno, L. A.; German, J. B.; Lebrilla, C. B. Method for the Identification of Lipid Classes Based on Referenced Kendrick Mass Analysis. *Anal. Chem.* **2010**, *82* (10), 4236−4245.
(52) May, J. C.; McLean, J. A. The Influence of Drift Gas Composition on the Separation Mechanism in Traveling Wave Ion Mobility Spectrometry: Insight from Electrodynamic Simulations. *Int. J. Ion Mobility Spectrom.* **2013**, *16* (2), 85−94.
(53) Laskin, J.; Denisov, E.; Futrell, J. A Comparative Study of Collision-Induced and Surface-Induced Dissociation. 1. Fragmentation of Protonated Dialanine. *J. Am. Chem. Soc.* **2000**, *122* (40), 9703−9714.
(54) McCormack, A. L.; Jones, J. L.; Wysocki, V. H. Surface-Induced Dissociation of Multiply Protonated Peptides. *J. Am. Soc. Mass Spectrom.* **1992**, *3* (8), 859−862.
(55) Cheng, C.; Gross, M. L. Applications and Mechanisms of Charge-Remote Fragmentation. *Mass Spectrom. Rev.* **2000**, *19* (6), 398−420.
(56) Wysocki, V. H.; Tsaprailis, G.; Smith, L. L.; Breci, L. A. Mobile and Localized Protons: A Framework for Understanding Peptide Dissociation. *J. Mass Spectrom.* **2000**, *35* (12), 1399−1406.
(57) Galhena, A. S.; Jones, C. M.; Wysocki, V. H. Influence of Cluster Size and Ion Activation Method on the Dissociation of Cesium Iodide Clusters. *Int. J. Mass Spectrom.* **2009**, *287* (1−3), 105−113.

https://doi.org/10.1021/jasms.3c00319
J. Am. Soc. Mass Spectrom. 2024, 35, 214−223